

Anisotropic thermoelectric transport properties in polycrystalline $SnSe_2$

Caiyun Li(李彩云), Wenke He(何文科), Dongyang Wang(王东洋), and Li-Dong Zhao(赵立东)
Citation: Chin. Phys. B, 2021, 30 (**6**): 067101. DOI: 10.1088/1674-1056/abeee1
Journal homepage: http://cpb.iphy.ac.cn; http://iopscience.iop.org/cpb

What follows is a list of articles you may be interested in

Intercalation of van der Waals layered materials: A route towards engineering of electron correlation

Jingjing Niu(牛晶晶), Wenjie Zhang(章文杰), Zhilin Li(李治林), Sixian Yang(杨嗣贤), Dayu Yan(闫大禹), Shulin Chen(陈树林), Zhepeng Zhang(张哲朋), Yanfeng Zhang(张艳锋), Xinguo Ren(任新国), Peng Gao(高鹏), Youguo Shi(石友国), Dapeng Yu(俞大鹏), Xiaosong Wu(吴孝松)
Chin. Phys. B, 2020, 29 (**9**): 097104. DOI: 10.1088/1674-1056/abab85

Vanadium based XVO_3 (X=Na, K, Rb) as promising thermoelectric materials: First-principle DFT calculations

N A Noor, Nosheen Mushahid, Aslam Khan, Nessrin A. Kattan, Asif Mahmood, Shahid M. Ramay
Chin. Phys. B, 2020, 29 (**9**): 097101. DOI: 10.1088/1674-1056/ab99ad

Single crystal growth, structural and transport properties of bad metal $RhSb_2$

D S Wu(吴德胜), Y T Qian(钱玉婷), Z Y Liu(刘子懿), W Wu(吴伟), Y J Li(李延杰), S H Na(那世航), Y T Shao(邵钰婷), P Zheng(郑萍), G Li(李岗), J G Cheng(程金光), H M Weng(翁红明), J L Luo(雒建林)
Chin. Phys. B, 2020, 29 (**3**): 037101. DOI: 10.1088/1674-1056/ab696e

Magnetism, optical, and thermoelectric response of $CdFe_2O_4$ by using DFT scheme

Q Mahmood, M Yaseen, K C Bhamu, Asif Mahmood, Y Javed, Shahid M Ramay
Chin. Phys. B, 2018, 27 (**3**): 037103. DOI: 10.1088/1674-1056/27/3/037103

Theoretical design of multifunctional half-Heusler materials based on first-principles calculations

Xiuwen Zhang(张秀文)
Chin. Phys. B, 2018, 27 (**12**): 127101. DOI: 10.1088/1674-1056/27/12/127101

Anisotropic thermoelectric transport properties in polycrystalline $SnSe_2$*

Caiyun Li(李彩云), Wenke He(何文科), Dongyang Wang(王东洋), and Li-Dong Zhao(赵立东)†

School of Materials Science and Engineering, Beihang University, Beijing 100191, *China*

(Received 2 March 2021; revised manuscript received 12 March 2021; accepted manuscript online 16 March 2021)

It is reported that $SnSe_2$ consisting of the same elements as SnSe, is a new promising thermoelectric material with advantageous layered structure. In this work, the thermoelectric performance of polycrystalline $SnSe_2$ is improved through introducing SnSe phase and electron doping (Cl doped in Se sites). The anisotropic transport properties of $SnSe_2$ are investigated. A great reduction of the thermal conductivity is achieved in $SnSe_2$ through introducing SnSe phase, which mainly results from the strong $SnSe_2$–SnSe inter-phase scattering. Then the carrier concentration is optimized via Cl doping, leading to a great enhancement of the electrical transport properties, thus an extraordinary power factor of ~5.12 $\mu W \cdot cm^{-1} \cdot K^{-2}$ is achieved along the direction parallel to the spark plasma sintering (SPS) pressure direction ($\parallel P$). Through the comprehensive consideration on the anisotropic thermoelectric transport properties, an enhanced figure of merit ZT is attained and reaches to ~ 0.6 at 773 K in $SnSe_2$-2% SnSe after 5% Cl doping along the $\parallel P$ direction, which is much higher than ~ 0.13 and ~ 0.09 obtained in $SnSe_2$-2% SnSe and pristine $SnSe_2$ samples, respectively.

Keywords: thermoelectric, $SnSe_2$, anisotropic structure, Cl-doping

PACS: 71.15.–m, 72.15.Cz, 72.20.Pa, 72.80.Rj **DOI:** 10.1088/1674-1056/abeee1

1. Introduction

Thermoelectric material, as the main body of device for reversible conversion between waste heat and electricity, can effectively alleviate the shortage of traditional primary energy and improve the situation of environmental degradation.[1,2] The dimensionless figure of merit (ZT) can be used to assess the conversion ability of thermoelectric materials for practical production and application, defined as $ZT = S^2\sigma T/\kappa_{tot}$, where S, σ, κ_{tot}, and T are the Seebeck coefficient, electrical conductivity, total thermal conductivity, and absolute temperature, respectively.[3–5] In recent years, a series of new theories and advanced material fabrication technologies have been developed to optimize the thermoelectric properties,[6–16] such as raising power factor ($PF = S^2\sigma$) through employing the band structure engineering[7,8,17] or lowering thermal conductivity by adopting defect engineering.[11,18–23] In addition, a certain material with low intrinsic thermal conductivity is explored to evade election–phonon coupling effectively.[14,24–27]

As a compound consisting of the same elements as SnSe, $SnSe_2$ has attracted much attention owing to not only its features of nontoxicity, non-pollution, earth-abundant, and low cost,[28] but also its natural layered structure leading to a low thermal conductivity,[29] making it become a competitive material in the field of thermoelectricity. Moreover, the first-principles calculations forecasted that $SnSe_2$ is able to reach a promising ZT value of ~ 2.95 in n-type $SnSe_2$ crystals when the carrier concentration (n) is raised to $\sim 10^{20}$ cm^{-3} at 800 K.[30] $SnSe_2$ is crystallized in a typical structure of CdI_2 (Figs. 1(a)–1(c)), and Se accumulates in a densely arranged hexagonal form while Sn is in the octahedral interstice surrounded by six Se atoms.[31] Similar to many layered compounds (Bi_2Se_3, Bi_2Te_3, etc.),[32] n-type polycrystalline $SnSe_2$ exhibits anisotropic thermoelectric properties along the a-axis and c-axis,[33] the weaker van der Waals chemical bonding between the layers makes the acoustic phonon mode along the c-axis softer than that along the a-axis, and results in a much lower thermal conductivity along the interlayer direction (c-axis).[34] When sintering the polycrystalline $SnSe_2$ samples, the layered structures are inclined to distribute along the sintering pressure direction. Therefore, superior ZT values are generally obtained along the pressuring direction owing to the much lower thermal conductivity.[18,30,33]

Among the diverse approaches for optimizing $SnSe_2$, the substitution of halogen atoms in Se sites is proved to be a convenient and highly effective strategy to increase the carrier concentration, and thus improves its electrical performance.[29,33,35–37] Shu *et al.* reported a high ZT of ~ 0.56 at 773 K in n-type polycrystalline $SnSe_2$ as the doping concentration of Cl reaches to $\sim 6\%$.[36] Further, Liu *et al.* built an imbedded Ag^+ bridge in the layers of $SnSe_2$ and harvested a record-breaking ZT of ~ 1.03.[18] However, the

*Project supported by the Beijing Natural Science Foundation, China (Grant No. JQ18004), the National Key Research and Development Program of China (Grant Nos. 2018YFA0702100 and 2018YFB0703600), the National Natural Science Foundation of China (Grant No. 51772012), Shenzhen Peacock Plan Team (Grant No. KQTD2016022619565991), and 111 Project (Grant No. B17002). This work was also supported by the National Postdoctoral Program for Innovative Talents, China (Grant No. BX20200028) and the high performance computing (HPC) resources at Beihang University. L.D.Z. thanks for the support from the National Science Fund for Distinguished Young Scholars (Grant No. 51925101).

†Corresponding author. E-mail: zhaolidong@buaa.edu.cn

© 2021 Chinese Physical Society and IOP Publishing Ltd

excessive increment of carrier concentration in the $SnSe_2$ matrix will inevitably result in a higher thermal conductivity from the electron contribution. In this case, we first introduce SnSe phase into $SnSe_2$ to reduce the lattice thermal conductivity because of the inter-phase scattering between $SnSe_2$ matrix and the second phases.[38–41] Subsequently, we select Cl dopant to optimize the carrier concentration and improve the electrical performance. Meanwhile, the anisotropic thermoelectric transport properties are investigated and analyzed in $SnSe_2$-based samples. We find a ~ 3 times lower thermal conductivity along the direction parallel to the spark plasma sintering (SPS) pressure ($\parallel P$), and a ~ 2 times higher PF along the direction perpendicular to the SPS pressure ($\perp P$) in $SnSe_2$-based samples. As a result, comprehensive consideration on the electrical properties and thermal conductivity, a higher ZT is attained along the $\parallel P$ direction. Besides, the minimum thermal conductivity decreases from ~ 0.57 $W{\cdot}m^{-1}{\cdot}K^{-1}$ to ~ 0.39 $W{\cdot}m^{-1}{\cdot}K^{-1}$ after introducing 2% SnSe along the $\parallel P$ direction. Then, the maximum PF yields a sharp increase in $SnSe_2$-2% SnSe after 5% Cl doping, which increases from ~ 1.70 $\mu W{\cdot}cm^{-1}{\cdot}K^{-2}$ to ~ 9.76 $\mu W{\cdot}cm^{-1}{\cdot}K^{-2}$ along the $\perp P$ direction. In the end, the ZT value is improved to as high as ~ 0.6 after the two-step optimization along the $\parallel P$ direction. All above optimizing processes are summarized in Fig. 2.

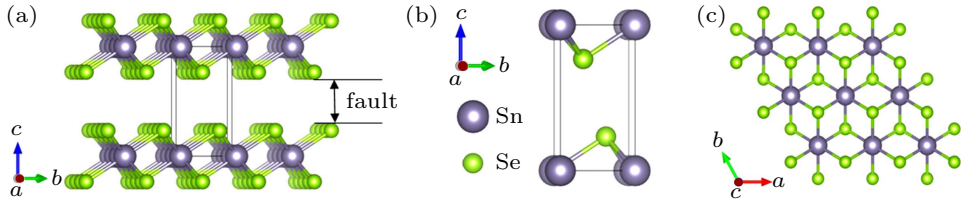


Fig. 1. Crystal structure of $SnSe_2$: (a) crystal structure along the a-axis; (b) the unit cell; (c) crystal structure along the c-axis.

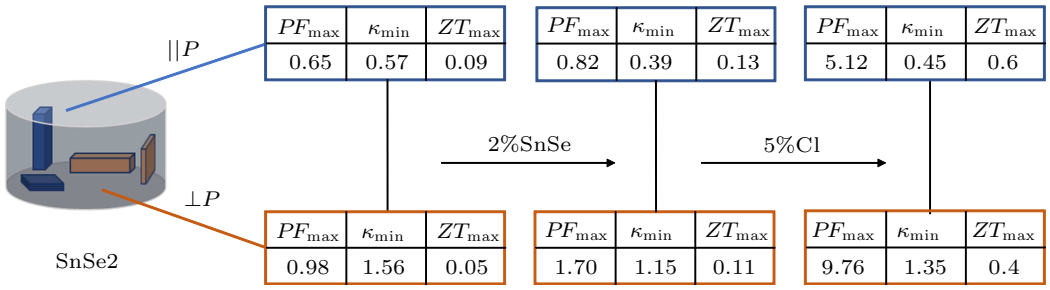


Fig. 2. A two-step optimization process for $SnSe_2$ along the $\parallel P$ and $\perp P$ directions. The units of PF_{max} and κ_{min} are $\mu W{\cdot}cm^{-1}{\cdot}K^{-2}$ and $W{\cdot}m^{-1}{\cdot}K^{-1}$, respectively.

2. Results and discussion

The powder XRD patterns of the $SnSe_2$-x% SnSe composites ($x = 0$, 1, 2, 3) are shown in Fig. 3(a). It is found that the diffraction peaks are well consistent with the simulated pattern (PDF# 01-089-2939). The lattice parameters do not change after adding 1% SnSe whatever the addition of SnSe content, which indicates the presence of SnSe phase (Fig. 3(b)). From the band gap measurement results (Figs. 3(c) and 3(d)), the band gap slightly decreases after adding SnSe into $SnSe_2$, which is due to the relative low band gap of SnSe.

The electrical conductivities of $SnSe_2$-x% SnSe samples along the two directions ($\parallel P$ and $\perp P$) are measured in the temperature range from 300 K to 773 K (Figs. 4(a) and 4(b)). The electrical conductivity is very low at room temperature and then increases as the temperature rises, which is a typical temperature-dependent intrinsic semiconductor feature. The electrical conductivity depends weakly on the temperature from 300 K to 600 K. At high temperatures, the electrical conductivity after adding SnSe is higher than that of pristine $SnSe_2$, which may come from that the reduced band gap from introducing SnSe is more conducive to thermal excitation as the temperature rises. This behavior is more striking along the $\perp P$ direction in this layered compound. It is obvious that the electrical conductivity along the $\perp P$ direction is superior to that along the $\parallel P$ direction, which indicates an outstanding $\perp P$ direction (can be considered as the in-plane direction in crystals) electrical transport property in $SnSe_2$. Besides, the Seebeck coefficients of all samples are relatively large and maintain within the range of ~ -400 $\mu V{\cdot}K^{-1}$ to -600 $\mu V{\cdot}K^{-1}$ at the whole working temperature (Figs. 4(c) and 4(d)). As a consequence, the power factors after introducing SnSe are higher than that of pristine $SnSe_2$, especially in the polycrystalline samples along the $\perp P$ direction (Figs. 4(e)–4(f)). A maximum power factor of ~ 1.7 $\mu W{\cdot}cm^{-1}{\cdot}K^{-2}$ at 773 K is attained in $SnSe_2$ along the $\perp P$ direction, and is twice of that along the $\parallel P$ direction, which is ascribed to the excellent in-plane carrier mobility in $SnSe_2$.

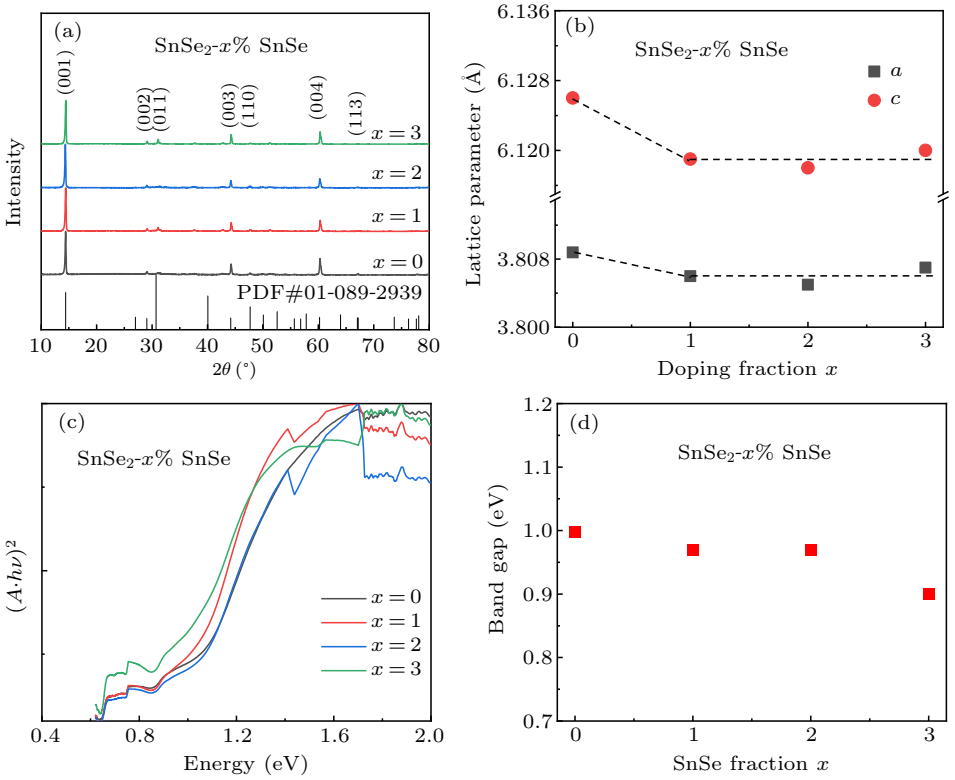


Fig. 3. (a) XRD patterns; (b) the lattice parameters; (c) UV–vis absorption spectra, and (d) band gaps for $SnSe_2$-x% SnSe.

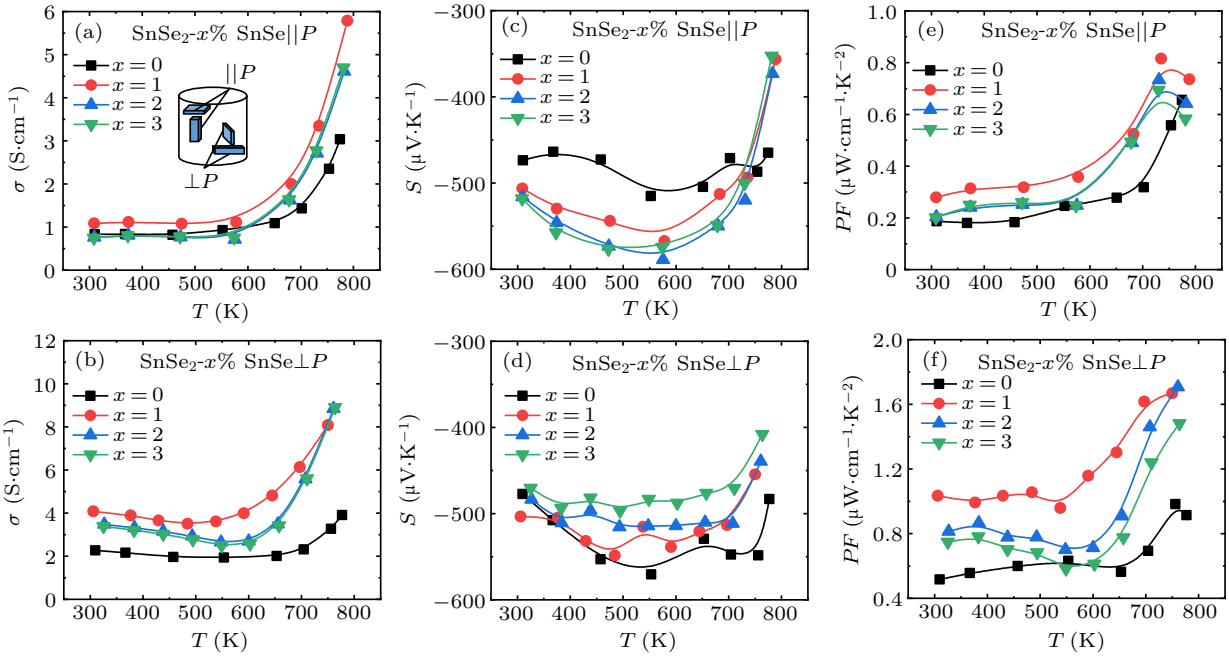


Fig. 4. Temperature dependence of electrical transport properties along the $\parallel P$ and $\perp P$ directions for $SnSe_2$-2% SnSe: (a)–(b) electrical conductivities; (c)–(d) Seebeck coefficients; (e)–(f) power factors.

To further investigate the difference in electrical properties after adding SnSe and along the two directions in $SnSe_2$, the Hall measurements are conducted. Since SnSe is a p-type phase in $SnSe_2$, the room-temperature (RT) carrier concentration decreases from $\sim 1.17 \times 10^{18}$ cm^{-3} to $\sim 5.62 \times 10^{17}$ cm^{-3}, but a high carrier mobility (μ) is obtained from ~ 1.82 cm^2·V^{-1}·s^{-1} to ~ 8.16 cm^2·V^{-1}·s^{-1} and ~ 10.57 cm^2·V^{-1}·s^{-1} to ~ 38.05 cm^2·V^{-1}·s^{-1} along the $\parallel P$ and $\perp P$ directions, respectively (Figs. 5(a) and 5(b)). The carrier mobilities along these two directions also show a significant distinction, the values along the $\perp P$ direction are $\sim$ 5–10 times higher than those along the $\parallel P$ direction. Based on the single parabolic band model,[42] we have calculated the carrier mobility as a function of carrier concentration (Fig. 5(c)). All the experimental data are under the simulated curve, which is attributed to the more complex scattering mechanism in

polycrystalline samples, such as grain boundary, precipitated phase, etc.[39,43] Moreover, on the basis of the single band model, the Seebeck coefficient can be obtained as[44,45]

$$S = \frac{8\pi^2 k_B^2}{3eh^2} m^* T \left(\frac{\pi}{3n}\right)^{2/3}, \quad (1)$$

where k_B represents the Boltzmann constant, h represents the Planck constant, and m^* represents the density of state effective mass. The Pisarenko line shows that the effective masses along the two directions are almost unchanged after increasing the SnSe concentration, indicating a single band transport feature at low carrier concentration in $SnSe_2$ (Fig. 5(d)).

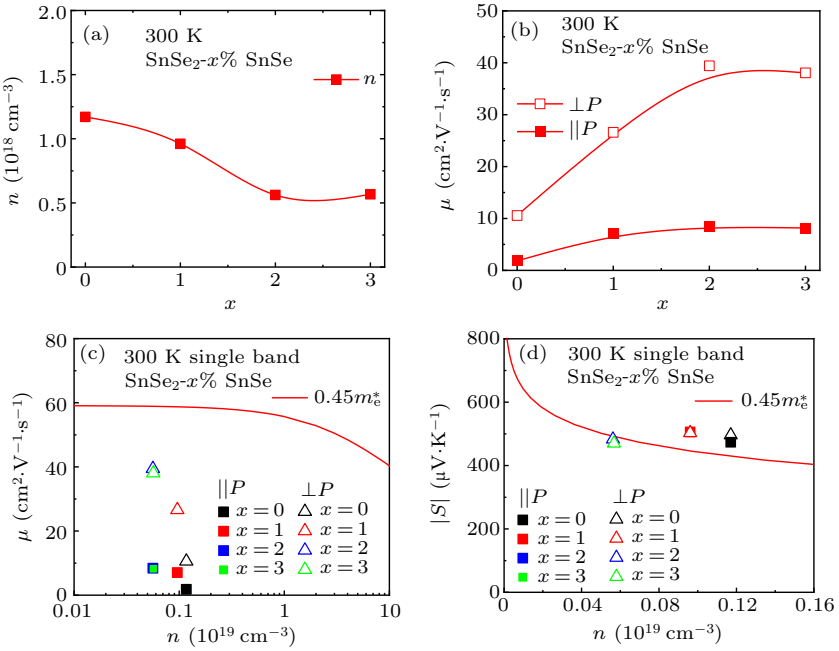


Fig. 5. (a) Carrier concentration; (b) carrier mobility; (c) carrier mobility, and (d) Seebeck coefficient as a function of carrier concentration along the $\parallel P$ and $\perp P$ directions for $SnSe_2$-x% SnSe.

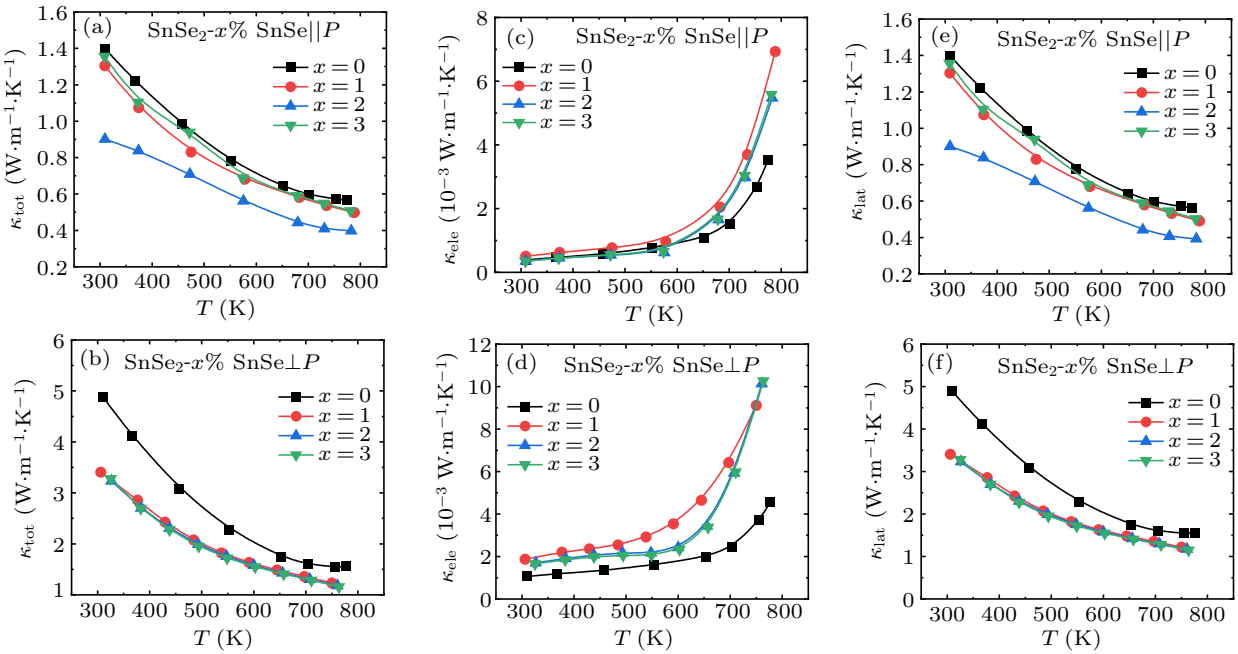


Fig. 6. The temperature dependence of thermal conductivity along the $\parallel P$ and $\perp P$ directions for $SnSe_2$-2% SnSe: (a)–(b) total thermal conductivity; (c)–(d) electronic thermal conductivity; (e)–(f) lattice thermal conductivity.

The total thermal conductivity (κ_{tot}) for all samples continuously decreases with elevating temperature (Figs. 6(a) and 6(b)). It can be seen that the κ_{tot} with SnSe phase along the $\parallel P$ and $\perp P$ directions are lower than those of pristine $SnSe_2$. Besides, the κ_{tot} along the $\parallel P$ direction is much lower than that along the $\perp P$ direction. The κ_{tot} mainly comes from the contributions of electronic thermal conductivity (κ_{ele}) and lattice thermal conductivity (κ_{lat}). The κ_{ele} is calculated by

$\kappa_{ele} = L\sigma T$, where L is the Lorentz constant, the κ_{ele} increases as temperature rises, which is mainly due to the increased electrical conductivity at high temperatures (Figs. 6(c) and 6(d)). The lattice thermal conductivity (κ_{lat}) can be obtained by subtracting κ_{ele} from κ_{tot}, namely, $\kappa_{lat} = \kappa_{tot} - \kappa_{ele}$. Interestingly, the overall κ_{lat} along the $\parallel P$ direction is ~ 3 times lower than that along the $\perp P$ direction (Figs. 6(e) and 6(f)). Moreover, a low κ_{lat} of ~ 0.39 W·m^{-1}·K^{-1} is obtained at 773 K in $SnSe_2$-2% SnSe sample along the $\parallel P$ direction while the κ_{lat} in the pristine $SnSe_2$ sample is ~ 0.56 W·m^{-1}·K^{-1}, implying a strong inter-phase scattering after introducing 2% SnSe.

In order to further explore the decline of the lattice thermal conductivity, we calculate the Grüneisen constant (γ) of these two samples along the $\parallel P$ direction,[46,47] as shown in Table 1. The γ of these two samples are ~ 3.03 and ~ 2.95, respectively, which indicates that the sample with 2% SnSe has a stronger anharmonicity.

Table 1. The longitude sound velocity (v_l), shear sound velocity (v_s), average sound velocity (v_a), and Grüneisen parameters (γ) of $SnSe_2$ and $SnSe_2$-2% SnSe.

	v_l (m/s)	v_s (m/s)	v_a (m/s)	γ
$SnSe_2$	2407	1228	1637	2.95
$SnSe_2$-2% SnSe	1947	959	1287	3.03

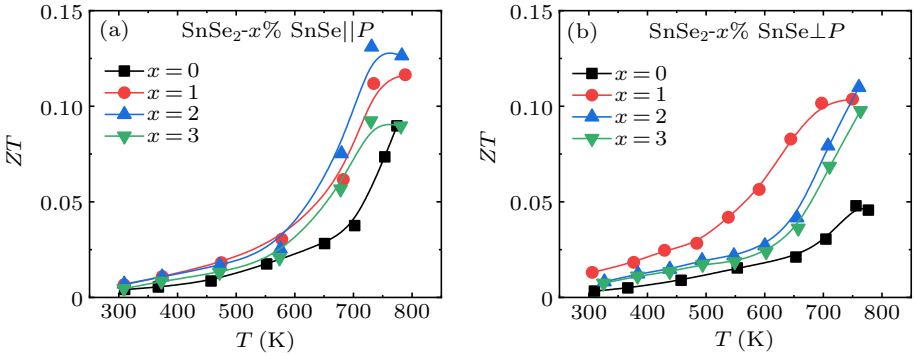


Fig. 7. Temperature dependent ZT values along the (a) $\parallel P$ and (b) $\perp P$ directions for $SnSe_2$-2% SnSe.

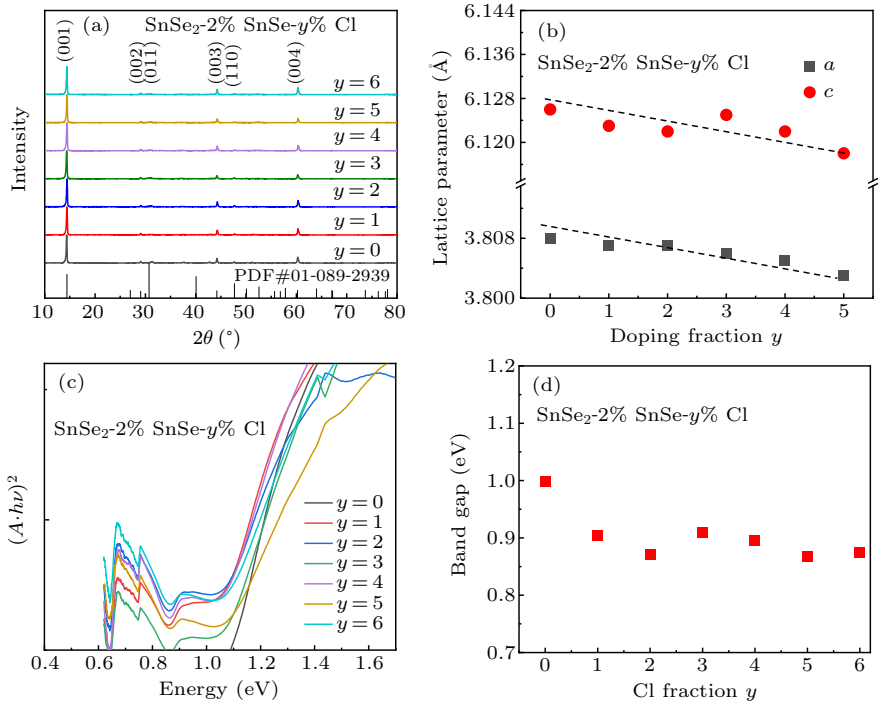


Fig. 8. (a) XRD patterns; (b) lattice parameters; (c) UV–vis absorption spectra, and (d) band gap for $SnSe_2$-2% SnSe-y% Cl.

Compared with the excellent electrical transport properties along the $\perp P$ direction, the contribution from thermal conductivity along the $\parallel P$ direction to final ZTs is more strikingly, especially when introducing SnSe phase with intrinsically low κ_{lat}. Therefore, combining the electrical and thermal properties along the two directions, relatively higher ZTs are achieved along the $\parallel P$ direction (Figs. 7(a) and 7(b)). The ZT value along the $\parallel P$ direction approaches to as high as ~ 0.13 at 773 K for $SnSe_2$-2% SnSe while is only ~ 0.09 for $SnSe_2$.

Based on the obtained low thermal conductivity and high ZT in $SnSe_2$ with 2% SnSe, we further improve the electrical transport properties through halogen element doping. The

XRD data of all samples with Cl doping are shown in Fig. 8(a). It is obvious that all the diffraction peaks agree well with the simulated pattern (PDF# 01-089-2939) ($SnSe_2$-2% SnSe-y% Cl, $y = 0$, 1, 2, 3, 4, 5, 6). Figure 8(b) shows that the lattice parameter gradually decreases with increasing Cl content, it proves that Cl is doped into $SnSe_2$ matrix as Cl has a smaller atomic radius than Se. The decrement of band gap from $\sim$ 1.0 eV to $\sim$ 0.83 eV is likely related to the introduction of impurity energy levels after Cl doping (Figs. 8(c) and 8(d)).

After Cl doping, the carrier concentration is optimized, leading to a huge increment of electrical conductivity (σ) in $SnSe_2$-2% SnSe samples. At room temperature, the σ increases from $\sim$4 S·cm^{-1} to $\sim$78 S·cm^{-1} and from $\sim$9 S·cm^{-1} to $\sim$ 208 S·cm^{-1} along the $\parallel P$ and $\perp P$ directions after 5% Cl doping, respectively (Figs. 9(a) and 9(b)). This striking difference mainly derives from the unique layered structure of $SnSe_2$ as mentioned above. The Seebeck coefficient decreases after increasing carrier concentration along the two directions (Figs. 9(c) and 9(d)). Besides, it can be seen that the PF reaches to as high as $\sim$ 5.12 μW·cm^{-1}·K^{-2} and $\sim$ 9.76 μW·cm^{-1}·K^{-2} after 5% Cl doping along the $\parallel P$ and $\perp P$ directions, respectively (Figs. 9(e) and 9(f)), which is an prominent enhancement compared to the undoped samples.

To further investigate the dramatic increase in the σ, the n and μ at room-temperature are measured. As Fig. 10(a) depicts, the n is largely enhanced from $\sim 5.6 \times 10^{17}$ cm^{-3} to $\sim 6.2 \times 10^{19}$ cm^{-3} after Cl doping, which benefits from the fact that Cl is an effective electron donor.[35] It is worth noting that the μ increases with rising the doping concentration from 1% to 5% (Fig. 10(b)), which may be due to the micro-regulation of Cl on $SnSe_2$ and SnSe phases.[36] In other word, Cl replaces Se not only in $SnSe_2$ but also in SnSe, making the SnSe phase be changed from intrinsic p-type to n-type, therefore, the n–p phase in $SnSe_2$ convert to n–n phase thus reducing the energy barrier between $SnSe_2$ and SnSe, which makes the carriers facilely migrate. As a consequence, the μ increases up to $\sim$ 12 cm^2·V^{-1}·s^{-1} after 5% Cl doping along the $\parallel P$ direction. Based on the single parabolic model,[42] experimental data locate under the simulated relationship curve of μ with increased n obviously (Fig. 10(c)), which is attributed to the dominance of grain boundary scattering in polycrystalline $SnSe_2$ at low temperatures.[48] Based on the Pisarenko relationship,[38,44] it is found that the effective mass increases after Cl doping (Fig. 10(d)), which implies a multiple band transport behavior in $SnSe_2$ as the carrier concentration rises.[35]

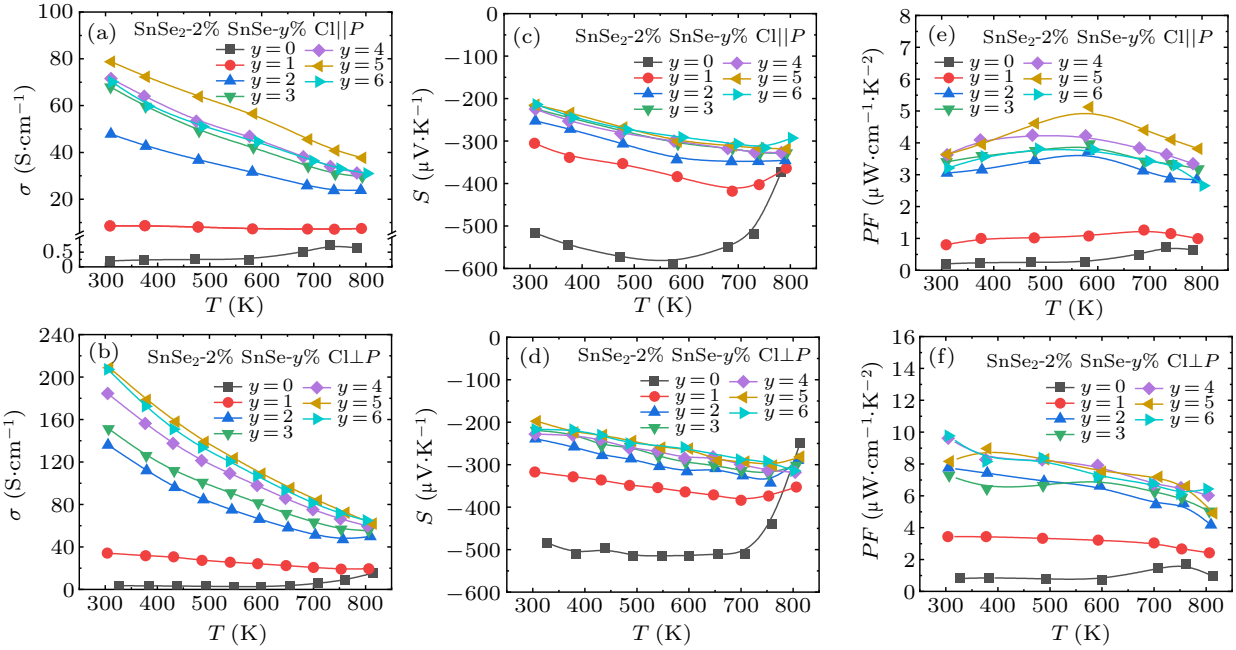


Fig. 9. The temperature dependence of electrical transport properties along the $\parallel P$ and $\perp P$ directions for $SnSe_2$-2% SnSe-y% Cl samples: (a)–(b) electrical conductivities; (c)–(d) Seebeck coefficients; (e)–(f) power factors.

It is found that the whole κ_{tot} after Cl doping are slightly higher compared to those of the undoped 2% SnSe samples, which are in the range of $\sim$ 0.45 W·m^{-1}·K^{-1} to $\sim$1.35 W·m^{-1}·K^{-1} at 773 K (Figs. 11(a) and 11(b)). Besides, the κ_{ele} increases rapidly with increasing the doping content owing to the contribution from the increased carrier concentration (Figs. 11(c)and 11(d)). In the end, the κ_{lat} increases slightly after Cl doping along the two directions, which may come from the reduced energy barrier between $SnSe_2$ and SnSe phases weakening the inter-phase scattering after Cl doping (Figs. 11(e) and 11(f)).

Through the comprehensive evaluation on the anisotropic electrical properties and thermal conductivity of $SnSe_2$-2% SnSe with Cl doping, the samples show higher ZT values

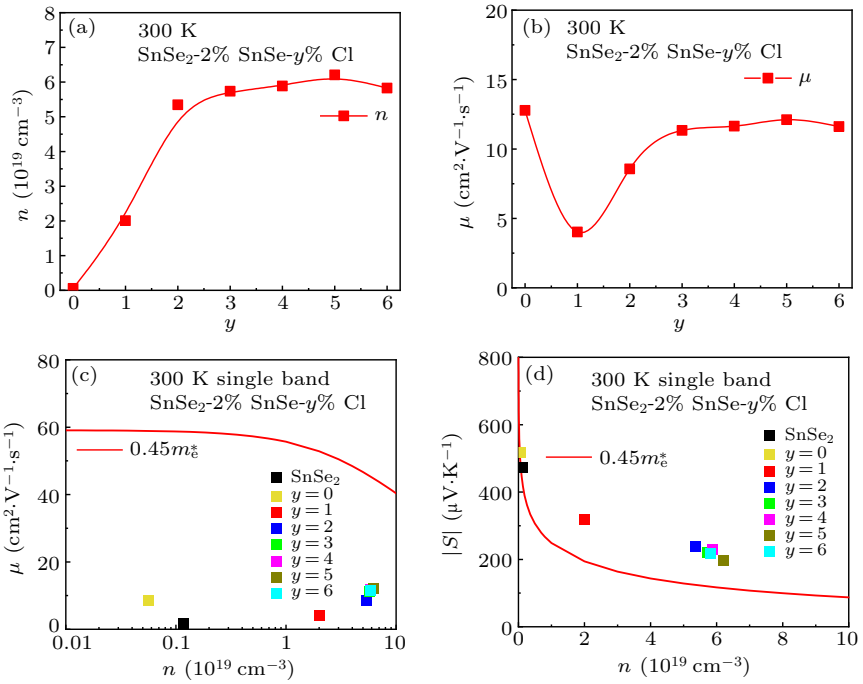


Fig. 10. (a) Carrier concentration; (b) carrier mobility; (c) carrier mobility, and (d) Seebeck coefficient as function of carrier concentration for $SnSe_2$-2% SnSe-y% Cl.

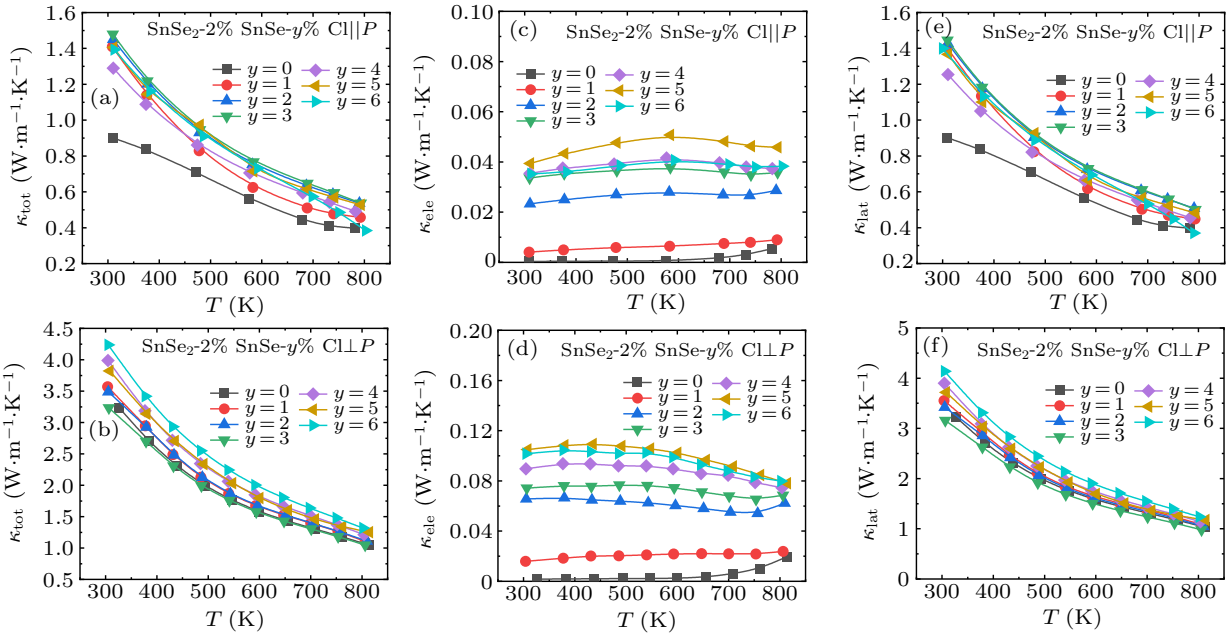


Fig. 11. The temperature dependence of thermal conductivities along the $\parallel P$ and $\perp P$ directions for $SnSe_2$-2% SnSe-y% Cl: (a)–(b) total thermal conductivities; (c)–(d) electronic thermal conductivities; (e)–(f) lattice thermal conductivities.

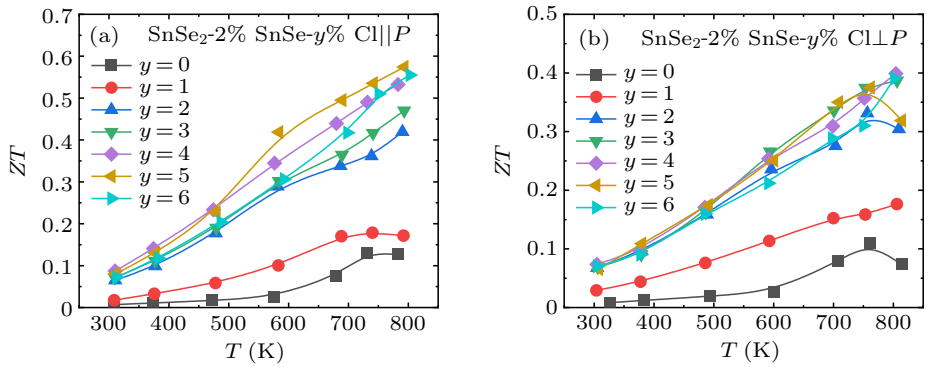


Fig. 12. Temperature dependent ZT values along the (a) $\parallel P$ and (b) $\perp P$ directions for $SnSe_2$-2% SnSe-y% Cl.

along the $\parallel P$ direction than the $\perp P$ direction (Figs. 12(a) and 12(b)). Finally, a maximum ZT of ~ 0.6 at 773 K is achieved in $SnSe_2$-2% SnSe-5% Cl along the $\parallel P$ direction, which is a great improvement compared to ZT of ~ 0.13 for the $SnSe_2$-2% SnSe sample without Cl doping.

2.1. Conclusion

In summary, the thermoelectric performance of $SnSe_2$ is improved successfully by a two-step optimization strategy, namely, reducing the thermal conductivity by introducing SnSe and then increasing the power factor through Cl doping. Specifically, introducing SnSe phase can significantly reduce the lattice thermal conductivity in $SnSe_2$ due to the inter-phase scattering and strong anharmonicity, then Cl doping optimizes the carrier concentration thus improving the electrical properties. Meanwhile, we also estimate that the anisotropic thermoelectric properties along the $\parallel P$ and $\perp P$ directions in $SnSe_2$-based samples, and find a more prominent contribution from the thermal conductivity to the final ZTs along the $\parallel P$ direction. Ultimately, a high ZT of ~ 0.6 along the $\parallel P$ direction is achieved for $SnSe_2$-2% SnSe-5% Cl sample at 773 K, which makes it a promising candidate for thermoelectric application.

References

[1] Zhao L D, Dravid V P and Kanatzidis M G 2014 *Energy Environ. Sci.* **7** 251
[2] Zhang X and Zhao L D 2015 *Journal of Materiomics* **1** 92
[3] Tan G, Zhao L D and Kanatzidis M G 2016 *Chem. Rev.* **116** 12123
[4] Wang Y N, Chen S P, Fan W H, Guo J Y, Wu Y C and Wang W X 2020 *Acta Phys. Sin.* **69** 246801 (in Chinese)
[5] Zheng L X, Hu J F and Luo J 2020 *Acta Phys. Sin.* **69** 247102 (in Chinese)
[6] Hsu K F, Loo S, Guo F, Chen W, Dyck J S, Uher C and Kanatzidis M G 2004 *Science* **303** 818
[7] Sfeir M Y, Beetz T, Wang F, *et al.* 2008 *Science* **312** 554
[8] Pei Y, Shi X, Lalonde A, Wang H, Chen L and Snyder G J 2011 *Nature* **473** 66
[9] Pei Y, Wang H and Snyder G J 2012 *Adv Mater* **24** 6125
[10] Biswas K, He J, Blum I D, Wu C I, Hogan T P, Seidman D N and Kanatzidis M G 2012 *Nature* **489** 414
[11] Li W, Zheng L, Ge B, Lin S, Zhang X, Chen Z and Pei Y 2017 *Adv. Mater.* **29** 17
[12] Zhao L D, Lo S H, Zhang Y, Sun H, Tan G, Uher C and Kanatzidis M G 2014 *Nature* **508** 373
[13] Zhao L D, Tan G, Hao S Q, He J Q, Pei Y L, Chi H, Wang H, Gong S K, Xu H B, Dravid V P, Uher C, Snyder G J, Wolverton C andKanatzidis M G 2015 *Science* **351** 141
[14] Chang C, Wu M, He D, *et al.* 2018 *Science* **360** 778
[15] Wu D, Pei Y, Wang Z, Wu H, Huang L, Zhao L D and He J 2014 *Advanced Functional Materials* **48** 7763
[16] Xiao Y and Zhao L D 2018 *npj Quantum Materials* **3** 1
[17] Xiao Y, Wang D, Zhang Y, Chen C, Zhang S, Wang K and Zhao L D 2020 *J. Am. Chem. Soc.* **142** 4051
[18] Liu C, Huang Z, Wang D, Wang X, Miao L, Wang X and Zhao L D 2019 *Journal of Materials Chemistry A* **7** 9761
[19] Huang Y, Zhou D, Chen X, Liu H, Wang C and Wang S 2016 *Chemphyschem* **17** 375
[20] Fu Li Z Z, Li Y W, Wang W T, Li J F, Li B, Zhoang A H, Luo J T and Fan P 2017 *Journal of Materials Science* **52** 10506
[21] Li J, Jia F, Zhang S, Zheng S, Wang B, Chen L and Wu L 2019 *Journal of Materials Chemistry A* **7** 19316
[22] Chen Z, Ge B, Li W, Lin S, Shen J, Chang Y and Pei Y 2017 *Nat. Commun.* **8** 13828
[23] Qu W W, Zhang X X, Yuan B F and Zhao L D 2017 *Rare Metals* **37** 79
[24] Qin B, Wang D, He W, Zhang Y, Wu H, Pennycook S J and Zhao L D 2019 *J. Am. Chem. Soc.* **141** 1141
[25] Chang C and Zhao L D 2018 *Materials Today Physics* **4** 50
[26] Wang D, Huang Z, Zhang Y, Hao L, Wang G, Deng S and Zhao L D 2020 *Science China Materials* **63** 1759
[27] Pei Y, Chang C, Wang Z, Yin M, Wu M, Tan G and Zhao L D 2016 *J. Am. Chem. Soc.* **138** 16364
[28] Yu P, Yu X, Lu W, Lin H, Sun L, Du K and Liu Z 2016 *Advanced Functional Materials* **26** 137
[29] Sun B Z, Ma Z, He C and Wu K 2015 *Phys. Chem. Chem. Phys.* **17** 29844
[30] Ding Y, Xiao B, Tang G and Hong J 2016 *The Journal of Physical Chemistry C* **121** 225
[31] Saha S, Banik A and Biswas K 2016 *Phys. Chem. Chem. Phys.* **17** 15634
[32] Zhou Y and Zhao L D 2017 *Adv. Mater.* **29** 1702676
[33] Wu Y, Li W, Faghaninia A, Chen Z, Li J, Zhang X and Pei Y 2017 *Materials Today Physics* **3** 127
[34] Zhou W X and Chen K Q 2015 *Sci. Rep.* **5** 15070
[35] Luo Y, Zheng Y, Luo Z, Hao S, Du C, Liang Q and Kanatzidis M G 2018 *Advanced Energy Materials* **8** 1702167
[36] Shu Y, Su X, Xie H, Zheng G, Liu W, Yan Y and Tang X 2018 *ACS Appl. Mater. Interfaces* **10** 15793
[37] Wu S, Liu C, Wu Z, Miao L, Gao J, Hu X and Zhou X 2019 *Ceramics International* **45** 82
[38] Qin B, Zhang Y, Wang D, Zhao Q, Gu B, Wu H and Zhao L D 2020 *J. Am. Chem. Soc.* **142** 5901
[39] Zhang X, Wang D, Wu H, Yin M, Pei Y, Gong S and Zhao L D 2017 *Energy & Environmental Science* **10** 2420
[40] Zhao L D, He J, Wu C I, Hogan T P, Zhou X, Uher C, Kanatzidis M G 2012 *J. Am. Chem. Soc.* **134** 7902
[41] Qin B C X, Zhou Y, Ming Y and Dong Z L 2018 *Rare Metals* **37** 343
[42] Pei Y, Gibbs Z M, Gloskovskii A, Balke B, Zeier W G and Snyder G J 2014 *Adv. Energy. Mater.* **4** 1400486
[43] He W K, Qin B C and Zhao L D 2020 *Chin. Phys. Lett.* **37** 087104
[44] Cutler M, Leavy J F and Fitzpatrick R L 1964 *Phys. Rev.* **133** A1143
[45] Toberer G S E 2008 *Nat. Mater.* **7** 105
[46] Xiao Y, Chang C, Pei Y, Wu D, Peng K, Zhou X and Zhao L D 2016 *Phys. Rev. B* **94** 125203
[47] Xiao Y, Wu H, Cui J, Wang D, Fu L, Zhang Y and Zhao L D 2018 *Energy Environ. Sci.* **11** 2486
[48] Schrade M, Berland K, Eliassen S N H, Guzik M N, Echevarria-Bonet C, Sorby M H and Finstad T G 2017 *Sci. Rep.* **7** 13760